sciendo

DOI: 10.2478/auoc-2022-0006

Ovidius University Annals of Chemistry Volume 33, Number 1, pp. 41 - 49, 2022

Entropy generation analysis in a gasket plate heat exchanger using non-spherical shape of alumina boehmite nanoparticles

Élcio NOGUEIRA*

Department of Mechanic and Energy, State University of Rio de Janeiro, Brazil

Abstract. The analysis deals with the thermo-hydraulic performance of a Gasket Plate Heat Exchanger used for cooling vegetable oils with a water-ethylene glycol 50% and volume fractions of non-spherical nanoparticles mixture as a refrigerant. The heat exchanger has 75 plates with a chevron angle equal to 30º. The Reynolds number of the refrigerant varies from 80 to 1530. The Reynolds number of the sunflower vegetable oil is fixed and equal to 30. The non-spherical nanoparticles used for analysis are platelet, cylindrical and brick types. Graphical results are presented for global heat transfer coefficient, heat capacity ratio, heat transfer rate, outlet temperatures, thermal and viscous entropy generation rate, and Bejan thermodynamic number. The results obtained allow us to conclude that it is possible to work with low relative flow rates using non-spherical nanoparticles, emphasizing platelet nanoparticles. The entropy generations analysis shows that very high flow rates of the refrigerant dissipate much of the energy in viscous form and do not contribute to oil cooling, with a consequent increase in the heat exchanger operating costs.

Keywords: plate heat exchanger; entropy generation; Bejan number; non-spherical nanoparticles; vegetable oil.

1. Introduction

This work aims to analyze the thermal and hydraulic performance of a gasket plate heat exchanger using an analytical procedure based on the second law of thermodynamics, emphasizing the entropy generation rate.

Gasket plate heat exchangers have small hydraulic diameters and undulations due to geometry, which leads to heat transfer enhancement. The relevant geometric aspects that influence the thermohydraulic behavior are the chevron angle, the surface enlargement factor, and the corrugation profile. Due to the importance of this type of heat exchanger in the industry, several numerical and analytical models have been developed in the last decades to describe its behavior and point out correction procedures that can lead to material savings and energy dissipation. With this objective, Neagu and Koncsag [1] present a correlation model to determine the Nusselt number that considers the energy losses caused by the reverse flow at the plates' edges change in the flow path associated with the chevron angle. The model is experimentally validated in an industrial facility with a chevron angle equal to 30º. Furthermore, they demonstrated using statistical analysis that the Nusselt correlation, calculated with generalized Lévêque correlation, presents results compatible with the experimental data obtained for the heat exchanger under investigation.

Different methods available in the literature make it possible to calculate the total pressure drop that occurs in a Gasket Plate Heat Exchanger. Neagu et al. [2] collected experimental data related to pressure drops in a vegetable oil refinery. They compared it with the correlations of Kumar, Muuley, and Buonopane & Troupe, cited in the published work on the conclusions they reached after the comparisons. They concluded that the results obtained by the different correlations present great dispersion among themselves and that the Kumar correlation results in oversizing. Therefore, they choose to use the other two correlations, with the prevalence of Mulley's, which carries information associated with the chevron tilt angle.

Skocilas and Palaziuk [3] developed a three-dimensional computational model to determine the heat transfer process in Gasket Plate Heat Exchanger in a turbulent regime. First, they determined values for heat transfer coefficient and heat loss. Then, they carried out a comparative analysis with experimental results obtained from the literature, considering the angle of ripple's inclination related to the main flow direction. Graphical research of temperature distribution shows heat exchanger regions with higher heat losses and low flow intensity. The main conclusion reached with the numerical simulation is that the results show an advantage in using chevron ripples as they promote higher heat transfer coefficients. Still, they promote an increase in hydraulic resistance and a higher pressure drop value.

Nogueira [4] uses the second law of thermodynamics and determines the thermal performance of a given Gasket Plate Heat Exchanger used for milk pasteurization and water as a refrigerant. The original heat exchanger has 20 plates. The developed work analyzed the effect of the variation in the number of plates on thermal performance. It presents thermal efficiency, effectiveness, entropy generation rate, and

* *E-mail address:* elcionogueira@hotmail.com

exit temperatures. Some of the conclusions he reached were: 1 - for a small number of plates, the effectiveness increases with the increase in the flow rate of the refrigerant; 2 - effectiveness tends to 1.0 when the number of plates approaches 80; 3 - for a high number of plates the relatively high-water flow rate has little influence on the thermal performance.

Kumar and Singh [5] present experimental work on a plate heat exchanger for Reynolds numbers ranging from 800 to 5900. They analyze the thermal and hydraulic performance of the heat exchanger using as parameters the Reynolds number, the power of pumping, the number of plates, and chevron tilt angle equal to 60º. The experimental Nusselt number is compared with correlations developed by Bassiouny-Martin and Wang-Sunden, referencing the presented work. In addition, they create correlations for Nusselt number and friction factor from the data obtained and the comparisons made. The main conclusion reached from the analysis is that uniform flow distribution for many plates should not be admitted.

Tovazhnyanskyy et al. [6] present a study related to the construction of special plates in Welded Plate Heat Exchanger. They create a model for analyzing a single-pass heat exchanger's thermal and hydraulic performance. Get expressions for determining the effectiveness and number of thermal units. The results were obtained to develop a model for a multi-pass heat exchanger. They validate the model from experimental data obtained in an industrial plant used to synthesize ammonia at high pressures. In addition, they developed a model that makes it possible to determine the height of the ripples and the number of passes required for specified operating conditions. They conclude by stating that heat exchangers with round plates specially developed for ammonia synthesis have higher thermal efficiency than traditional tubular heat exchangers.

Jamil et al. [7] present theories for heat exchanger design using the Exergoeconomic Method and Normalized Sensitivity Analysis Method. The first one deals with the joint application of economic and thermodynamic analysis and is more efficient than thermodynamic and financial analysis methods. The second allows a rational comparison between output and input parameters by normalizing the sensitivity coefficients by the nominal values. They validate the models experimentally in a plate heat exchanger used in a desalination system. Exergoeconomic method includes combinatorial effects of conventional methods.

Nguyen et al. [8] apply electrolytic coating technique to plate heat exchanger to improve thermo-hydraulic efficiency. They use nickel, copper, and silver on stainless steel plates using electrodeless galvanizing and perform a heat transfer experiment to evaluate the overall heat transfer coefficient, friction factor, number of transfer units, efficiency, and performance evaluation criteria. After coating, it goes from smooth to rough, changing the morphology of the surface. Coated plate heat exchangers show significant performance improvement, highlighting silver, followed by copper and nickel. They note that the primary factors for improved performance are increased surface area and the creation of turbulence associated with roughness. They conclude by stating that coated boards are suitable for working in corrosive environments.

Almurtaji [10] carried out a systematic review of heat exchanger technology and the use of nanofluids to improve thermo-hydraulic efficiency. One of the focuses of the work is plate heat exchangers. They present a discussion on thermophysical properties and emphasize the importance of nanofluids for future applications. They show extensive literature and conclude that CNT-based nanofluids are highly effective for improving thermal performance, especially in plate heat exchangers.

Timofeeva et al. [11] investigate the thermal conductivity and viscosity of various shapes of alumina nanoparticles in a mixture of water and ethylene glycol. They carry out an experiment and develop a theoretical model and observe that the presence of nanoparticles produces an effective increase in thermal conductivity as a function of interfacial effects proportional to the surface area. In addition, they keep that the presence of nanoparticles significantly increases the viscosity of the suspensions due to structural restrictions. However, they demonstrate that it is possible to reduce the viscosity of the alumina nanofluid by adjusting its pH without affecting the thermal conductivity. Furthermore, they use the experimental values obtained for thermal conductivity and viscosity to analyze the efficiency of nanofluids in laminar and turbulent regimes in real applications. Finally, they emphasize that the evaluation of nanofluids requires an understanding of their characteristics and thermophysical properties.

Matsegora et al. [12] present an approach to determine the influence of the wave geometry on the plate heat exchanger under fouling conditions. They use a dimensionless scale model and discuss the effect of the plate corrugation geometry on the performance of the heat exchanger used for fine heating broth in a sugar plant. They consider that the slope angle of the ripples is the main influencing factor and show its effect on the incrustation intensity. They discuss measures to mitigate the impact of surges on incrustation. They point out that plates with higher angles of inclination may be preferable in conditions of water fouling but emphasize that the decision depends on the accurate modeling of the process and economic factors.

Warlo et al. [13] report that they have worked for years to develop and characterize heat exchangers. They have recently included the analysis of fouling behavior in performance optimization design. They present experimental results for four different applications and compare thermodynamic performance in terms of fouling by airside $CaCO_3$ particle crystallization in different test facilities. The effect of fouling is investigated in a wet cooling tower on a laboratory scale and applied to real systems. They conclude that heat exchangers' drop in thermodynamic performance can be characterized through integral methods.

Garcia Rojas et al. [14] obtained data to determine the physical properties of vegetable oils used in the processed food industry. The vegetable oils analyzed are cotton, canola, sunflower, and corn. They measured thermal conductivity, viscosity, specific heat, and density for temperature variations ranging from 26 ºC to

160 ºC and observed that the properties are influenced by temperature. In addition, they developed correlations for the properties within the studied temperature range. They report that the developed correlations adequately fit the experimental results.

2. Methodology

Gasket plate heat exchangers were used initially for the pasteurization of milk [4]. However, they have been used in almost all industry branches because of their versatility and excellent thermal performance. Figure 1 presents a view of the components used in one of these heat exchangers. Figure 2 shows the main component of the heat exchanger and, in this case, a particular type of plate that is frequently used in applications. The chevron plate has corrugations slope angle to create eddies in the flow and improve the heat exchange [1, 2].

The heat exchanger under analysis transports hot sunflower vegetable oil and exchanges heat with a water-ethylene glycol with volume fractions of non-spherical nanoparticles. The works carried out by Neagu et al. they are [2, 3] deal separately with the thermal [2] and hydrodynamic [3] aspects, making it possible to obtain the geometric and physical parameters of the heat exchanger. In addition, they provided equations for determining the Reynolds number and friction factor with tilt angle as a fundamental parameter. The theoretical and experimental analyses presented in the cited studies use a wide range of Reynolds numbers for the refrigerant fluid and serve as a reference for this work.

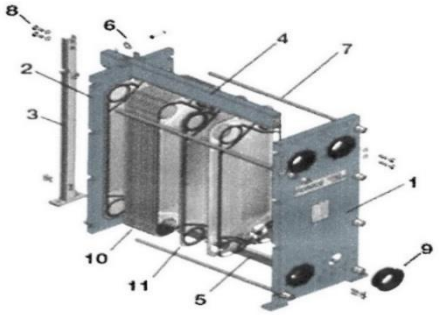

Figure 1. Exploded view of a typical Gasket Plate Heat Exchanger: 1 - fixed plate; 2 – pressure plate; 3 - support; 4 – carrying beam; 5 – lower plate guide; 6 – carrying roller; 7 – tightening bolt; 8 – fixing bolt; 9 - rubber liner; 10 - gasket; 11 - heat transfer plate.

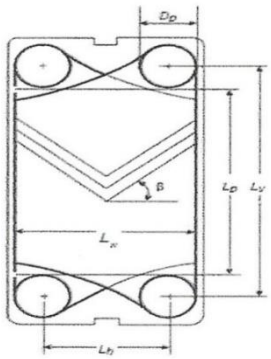

Figure 2. Main dimensions of chevron plate for the projected Gasket Plate Heat Exchanger

Primary data considered for the analysis are presented in Eq. 1-6:

$$Tc_i = 30\,º\,C \quad water - ethyleneglycol + nanoparticles \qquad (1)$$

$$Th_i = 110\,º\,C \quad sunflower\ vegetable\ oil \qquad (2)$$

$$\bar{T}c = 35\ º\,C \qquad (3)$$

$$\bar{T}h = 75\ º\,C \qquad (4)$$

$$T_W = 55\ º\,C \qquad (5)$$

Tc_i and Th_i are the inlet temperatures of water and vegetable oil.

$$N_t = 75 \qquad (6)$$

N_t is the number of plates.

The properties of sunflower vegetable oil are obtained through polynomial interpolations (Eq. 7-11) from tables presented in [14].

$$\rho_h = 920.8893939 - 0.09046037296\bar{T}_h - 0.00037121212\bar{T}_h{}^2 + 2.33100233110^{-6}\bar{T}_h{}^3 \ldots \qquad (7)$$

$$\mu_h = 0.144681007 - 0.00571479528\bar{T}_h + 9.8117277110^{-5}\bar{T}_h{}^2 - 7.88058566410^{-7}\bar{T}_h{}^3 + 2.40260780910^{-9}\bar{T}_h{}^4 \qquad (8)$$

$$\mu_W = 0.144681007 - 0.00571479528T_W + 9.8117277110^{-5}T_W{}^2 - 7.88058566410^{-7}T_W{}^3 + 2.40260780910^{-9}T_W{}^4 \qquad (9)$$

$$k_h = 0.1595212121 + 7.62626262610^{-5}\bar{T}_h - 5.30303030310^{-7}\bar{T}_h{}^2 + 2.525252510^{-9}\bar{T}_h{}^3 \qquad (10)$$

$$Cp_h = 2046.651515 + 3.511130536\bar{T}_h - 0.0056060606606\bar{T}_h{}^2 + 9.90675990710^{-6}\bar{T}_h{}^3 \qquad (11)$$

The equations used at the calculation of Prandtl number are (12-14) for the hot fluid and (21-23) for the cold one. Physical properties values of the fluids (17-20; 24-25) and their fouling factors (15-16) also serve to the following analysis:

$$\nu_h = \frac{\mu_h}{\rho_h} \quad m^2/s \qquad (12)$$

ν_h is the kinematic viscosity or momentum diffusivity of the sunflower oil.

$$\alpha_h = \frac{k_h}{\rho_h Cp_h} \quad m^2/s \qquad (13)$$

α_h is the thermal diffusivity of the sunflower oil.

$$Pr_h = \frac{\nu_h}{\alpha_h} \qquad (14)$$

Pr_h is the Prandtl number of the sunflower oil.

$$Rf_c = 0.00018\ W/(m^2K) \qquad (15)$$

$$Rf_h = 0.00053\ W/(m^2K) \qquad (16)$$

Rf_c and Rf_h are the fouling factor of the cold and hot fluids, respectively.

$$\rho_c = 1067.5\ kg/m^3\ water - ethyleneglycol50\% \qquad (17)$$

$$\mu_c = 3.3910^{-3}\ (kgs)/m\ water - ethyleneglycol50\% \quad (18)$$

$$k_c = 0.3799\ W/(mK)\ water - ethyleneglycol50\% \quad (19)$$

$$Cp_c = 3300\ J/(kgK)\ water - ethyleneglycol50\% \quad (20)$$

$$\nu_c = \frac{\mu_c}{\rho_c} \quad m^2/s \quad (21)$$

$$\alpha_c = \frac{k_c}{\rho_c Cp_c} \quad m^2/s \quad (22)$$

$$Pr_c = \frac{\nu_c}{\alpha_c} \quad (23)$$

$$\rho_{Particle} = 3050\ kg/m^3\ forBoehmiteAlu\,min\ a \quad (24)$$

$$Cp_{Particle} = 618.3\ J/(kgK)\ forBoehmiteAlu\,min\ a \quad (25)$$

Table 1 below was included in the article published by Monfared et al. [9] coefficients that characterize non-spherical nanoparticles concerning dynamic and thermal aspects. The coefficient C_k characterizes the thermal conductivity and the coefficients A_1 and A_2 characterize the dynamic viscosity. These coefficients are used in the present analytical model, to calculate the properties of nanofluids (Eq. 26-32).

Table 1. Coefficients that characterize the non-spherical shape of nanoparticles in dynamic viscosity and thermal conductivity [9]

Type	C_k	A_1	A_2
Platelets	2.61	37.1	612.6
Blades	2.74	14.6	123.3
Cylindrical	3.95	13.5	904.4
Bricks	3.37	1.9	471.4

The properties of the nanofluids are given by:

$$\mu_{nano} = \mu_c(1 + A_1\phi + A_2\phi^2) for\ non - spherical\ shape \quad (26)$$

$$\kappa_{nano} = k_c(1 + C_k\phi)\ for\ non - spherical\ shape \quad (27)$$

$$\rho_{nano} = \rho_{Particle}\phi + (1-\phi)\rho_c \quad (28)$$

$$Cp_{nano} = \frac{Cp_{Particle}\rho_{Particle}\phi + (1-\phi)Cp_c\rho_c}{\rho_{nano}} \quad (29)$$

Where: ϕ is the nanoparticle volume fraction.

$$\nu_{nano} = \frac{\mu_{nano}}{\rho_{nano}} \quad (30)$$

$$\alpha_{nano} = \frac{k_{nano}}{\rho_{nano} Cp_{nano}} \quad (31)$$

$$Pr_{nano} = \frac{\nu_{nano}}{\alpha_{nano}} \quad (32)$$

The geometrical dimensions of the gasket plate heat exchanger and the thermal conductivity of its manufacturing material are presented in (33-50):

$$L_V = 1.070\ m \quad (33)$$

L_V is the vertical distance between centers of ports.

$$L_p = 0.858\ m \quad (34)$$

L_p is the plate length between ports.

$$L_w = 0.450\ m \quad (35)$$

L_w is the plate width.

$$L_h = 0.238\ m \quad (36)$$

L_h is the horizontal length between centers of ports.

$$D_P = 0.212\ m \quad (37)$$

D_P is the port diameter.

$$\delta_W = 0.610^{-3}\ m \quad (38)$$

δ_W is the plate thickness.

$$k_W = 17.5\ W/(mK) \quad (39)$$

k_W is the thermal conductivity of the plate.

$$L_C = 175.5610^{-3}\ m \quad (40)$$

L_C is the compressed plate pack length.

$$Pit = \frac{L_c}{N_t} \quad (41)$$

Pit is the plate pitch.

$$b = Pit - \delta_W \quad (42)$$

b is the corrugation depth.

$$\varphi = 1.17 \quad (43)$$

φ is the surface enlargement factor.

$$D_h = \frac{2b}{\varphi} \quad (44)$$

D_h is the hydraulic diameter.

$$A_{ch} = bL_W \quad (45)$$

A_{ch} is the channel cross-sectional free flow area.

$$N_e = N_t - 3 \quad (46)$$

N_e is effective heat transfer number of plates.

$$N_p = 1 \quad (47)$$

N_p is the number of fluid passes.

$$N_{cp} = \frac{N_t - 1}{2N_p} \quad (48)$$

N_{cp} is the number of channels for one pass.

$$A_1 = 0.331m^2 \quad (49)$$

A_1 is the heat transfer area for a plate.

$$A_e = A_1 N_e \quad (50)$$

A_e is the heat transfer total area.

The analysis is made for a fixed value of Reynolds number on the hot fluid side (the vegetable oil) (Eq. 51):

$$Re_h = 30.0 \quad fixed \quad (51)$$

Re_h is the Reynolds number for hot fluid.

The Eq. 52-79 served to calculate Nusselt numbers, according to the modified Lévêque correlation [1]:

$$G_{ch} = \frac{Re_h\mu_h}{D_h} \quad (52)$$

G_{ch} is the mass velocity.

$$\dot{m}_{ch} = G_{ch}A_{ch} \quad (53)$$

$\dot{m}_{ch}$is the mass flow rate per channel

$$\dot{m}_h = \dot{m}_{ch} N_{c_p} \quad (54)$$

$\dot{m}_h$is the total mass flow rate of the hot fluid.

$$G_{cc} = \frac{Re_c \mu_{nano}}{D_h} \quad (55)$$

$$\dot{m}_{cc} = G_{cc} A_{ch} \quad (56)$$

$$\dot{m}_c = G_{cc} A_{ch} \quad (57)$$

$$C_c = \dot{m}_c Cp_{nano} \quad (58)$$

$$C_h = \dot{m}_h Cp_h \quad (59)$$

C_h is the thermal capacity of the hot fluid.

$$C^* = \frac{C_{min}}{C_{max}} \quad (60)$$

C_{min} is the minimum thermal capacity between the hot and cold fluids.

The methodology below, formulated by Neagu and Koncsag [1], introduces several parameters that explicitly depend on the angle of inclination of the chevron, emphasizing the Nusselt numbers.

$$l = Pit\, sin(\beta) \quad (61)$$

β is the chevron inclination angle and l is the corrugation wavelength.

$$L_{furr} = \frac{l}{sin(2\beta)} \quad (62)$$

$$L_{long} = \frac{l}{sin(\beta)} \quad (63)$$

L_{furr} and L_{long} are the furrow and longitudinal flow components.

$$XX = \frac{b}{Pit} \quad (64)$$

XX is the ratio corrugation depth.

$$D_{h\,sin\,e} = (0.149XX^3 - 0.623XX^2 + 1.087XX - 0.0014)l \quad (65)$$

$D_{h\,sin\,e}$ is the hydraulic dynamic diameter of a sine duct.

$$A_{ch\,sin\,e} = A_{ch}\, cos(\beta) \quad (66)$$

$A_{ch\,sin\,e}$ is the channel cross-section transverse to the furrow.

$$u_{sin\,ec} = \frac{\dot{m}_{cc}}{\rho_{nano} A_{ch\,sin\,e}} \quad (67)$$

$$u_{sin\,eh} = \frac{\dot{m}_{ch}}{\rho_h A_{ch\,sin\,e}} \quad (68)$$

$$Re_{sin\,ec} = \frac{2u_{sin\,ec} D_{h\,sin\,e}}{\nu_{nano}} \quad (69)$$

$$Re_{sin\,eh} = \frac{2u_{sin\,eh} D_{h\,sin\,e}}{\nu_h} \quad (70)$$

$$C = 2.6624XX^4 - 10.586XX^3 + 11.262XX^2 - 1.036XX + 9.6 \quad (71)$$

$$K_{e\,inf} = 5.888XX^4 + 9.4611XX^3 - 4.248XX^2 - 0.1333XX + 2.648 \quad (72)$$

$$K_{d\,inf} = 1.7237XX^4 + 2.7669XX^3 - 1.2651XX^2 - 0.0097XX + 1.512 \quad (73)$$

$$K_{inf} = 2(K_{e\,inf} - K_{d\,inf}) \quad (74)$$

$$B = \frac{K_{inf} D_{h\,sin\,e}}{4 l_{furr}} \quad (75)$$

$$f_{appc} = \frac{C}{Re_{sin\,ec}} + B \quad (76)$$

$$f_{apph} = \frac{C}{Re_{sin\,eh}} + B \quad (77)$$

f_{app} is the apparent friction coefficient.

$$Nu_c = 0.40377(4 f_{appc}\, Re^2_{sin\,ec} + Pr_{nano}(\frac{D_{h\,sin\,e}}{l_{furr}})^{1/3} \quad (78)$$

$$Nu_h = 0.40377(4 f_{apph}\, Re^2_{sin\,eh} + Pr_h \frac{D_{h\,sin\,e}}{l_{furr}})^{1/3} \quad (79)$$

The heat transfer partial coefficients on the hot fluid side and on the cold fluid side respectively, are calculated with Eq. 80-82, then the overall coefficient with Eq. 82, the number of transfer units (Eq. 83) and the thermal effectiveness (Eq. 84):

$$h_c = \frac{Nu_c k_{nano}}{D_{h\,sin\,e}} \quad (80)$$

$$h_h = \frac{Nu k_h}{D_{h\,sin\,e}} \quad (81)$$

$$Uo = \frac{1}{\frac{1}{h_c} + \frac{1}{h_h} + \frac{\delta_W}{k_W} + Rf_c + Rf_h} \quad (82)$$

$$NTU = \frac{UoA_e}{C_{min}} \quad (83)$$

$$\varepsilon_T = \frac{1 - e^{[-NTU(1-C^*)]}}{1 + C^* e^{[-NTU(1-C^*)]}} \quad (84)$$

ε_T is the thermal Effectiveness [15-16].

The heat transfer rate, thermal irreversibility and thermal entropy generation rate are calculated with Eq. 85-89.

$$\dot{Q} = \varepsilon_T C_{min}(Th_i - Tc_i) \quad (85)$$

$$Tc_o = Tc_i + \frac{\dot{Q}}{\dot{m}_c Cp_c} \quad (86)$$

$$Th_o = Th_i - \frac{\dot{Q}}{\dot{m}_h Cp_h} \quad (87)$$

$$\sigma_T = (\frac{C_h}{C_{min}})\, ln(\frac{Th_o}{Th_i}) + (\frac{C_{nano}}{C_{min}})\, ln(\frac{Tc_o}{Tc_i}) \quad (88)$$

σ_T is the thermal irreversibility.

$$\dot{S}_{genT} = \sigma_T C_{min} \quad (89)$$

$\dot{S}_{genT}$ is the thermal entropy generation rate [17-18].

The hydraulic methodology below, formulated by Neagu et al. [2], introduces parameters that explicitly depend on the chevron inclination angle, emphasizing the friction factor (Eq. 90-91):

$$f_c = (\frac{\beta}{30})^{0.83}[(\frac{30.2}{Re_c})^5 + (\frac{6.28}{Re_c})^{0.5}]^{0.2} \quad (90)$$

$$f_h = (\frac{\beta}{30})^{0.83}[(\frac{30.2}{Re_h})^5 + (\frac{6.28}{Re_h})^{0.5}]^{0.2} \quad (91)$$

f_c and f_h are the friction factors for cold and hot fluids, respectively.

The pressure drop, the outlet and inlet pressure are calculated with Eq. 92-102.

$$\Delta P_c = 4 f_c (\frac{L_P N_P}{D_h})(\frac{G^2_{cc}}{2\rho_{nano}})(\frac{\mu_{nano}}{\mu_W})^{-0.17} \quad (92)$$

$$\Delta P_h = 4f_h\left(\frac{L_p N_P}{D_h}\right)\left(\frac{G_{ch}^2}{2\rho_h}\right)\left(\frac{\mu_h}{\mu_W}\right)^{-0.17} \quad (93)$$

ΔP_h and ΔP_c are the pressure drops for hot and cold fluids, respectively.

$$G_{pc} = 4\left(\frac{\dot{m}_c}{\pi D_p^2}\right) \quad (94)$$

$$G_{ph} = 4\left(\frac{\dot{m}_h}{\pi D_p^2}\right) \quad (95)$$

G_{pc} and G_{ph} are the mass velocity for cold and hot fluids in the port.

$$\Delta P_{pc} = 1.4N_p\left(\frac{G_{pc}^2}{2\rho_{nano}}\right) \quad (96)$$

$$\Delta P_{ph} = 1.4N_p\left(\frac{G_{ph}^2}{2\rho_h}\right) \quad (97)$$

ΔP_{pc} and ΔP_{ph} are the pressure drops in the port duct.

$$\Delta t_c = \Delta P_c + \Delta P_{pc} \quad (98)$$

$$\Delta t_h = \Delta P_h + \Delta P_{ph} \quad (99)$$

$$P2_c = P2_h = P_{atm} \quad (100)$$

$P2_c$ and $P2_h$ are, by hypothesis, the outlet pressures. Then,

$$P1_c = P2_c + \Delta t_c \quad (101)$$

$$P1_h = P2_h + \Delta t_h \quad (102)$$

equations 103-106 lead to the value of Bejan thermodynamic number:

$$R = \frac{Th_i - Th_o}{Tc_o - Tc_i} \quad (103)$$

$$\sigma_f = -\left(\frac{C_h}{C_{min}}\right) R ln\left(\frac{P2_h}{P1_h}\right) - \left(\frac{C_{nano}}{C_{min}}\right) R\, ln\left(\frac{P2_c}{P1_c}\right) \quad (104)$$

$$\dot{S}_{genf} = \sigma_f C_{\min} \quad (105)$$

σ_f and $\dot{S}_{genf}$ are the viscous irreversibility and the viscous entropy generation rate.

Finally, we have:

$$Be = \frac{\dot{S}_{genT}}{\dot{S}_{genT} + \dot{S}_{genf}} \quad (106)$$

Be is the Bejan thermodynamic number [19-20].

3. Results and discussion

The global heat transfer coefficient versus Reynolds number in the range from 80 to 1530 and volume fraction of nanoparticle equal 0.5% is presented in Figure 3. It is possible to observe a considerable variation in global heat transfer in the range of the Reynolds number under analysis. However, due to the low volume fraction, it is impossible to observe nanoparticles' influence. When the volume fraction of the nanoparticles grows to 2.0%, Figure 4, the effect becomes evident, and the non-spherical nanoparticle that presents higher values for the global heat transfer coefficient is the Brick Boehmite Alumina.

Figures 5 and 6 show results for heat transfer rate as a function of a wide range of Reynolds numbers for volume fractions of nanoparticles equal to 0.5% and 2.0%, respectively. In these cases, it is possible to observe more clearly the influence of nanoparticles, notably for low Reynolds numbers. In contrast to the result observed for the global heat transfer coefficient, the non-spherical nanoparticle that presents the highest heat transfer rate is the Platelet type. This fact, without further analysis, can lead to hasty conclusions.

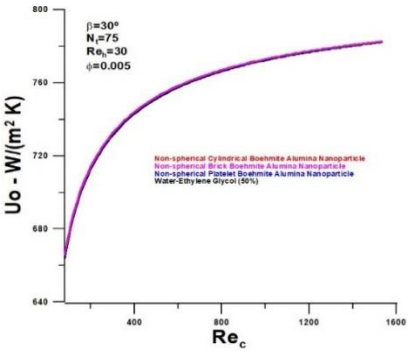

Figure 3. Global heat transfer coefficient versus Reynolds number with volume fraction of nanoparticles equals 0.5% as parameters

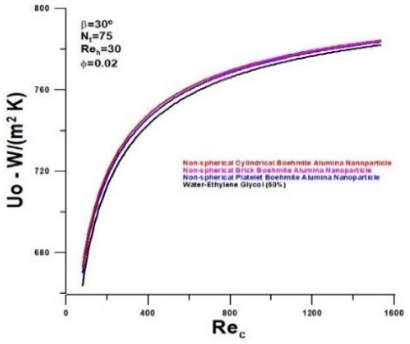

Figure 4. Global heat transfer coefficient versus Reynolds number with volume fraction of nanoparticles equal 2.0% as parameters

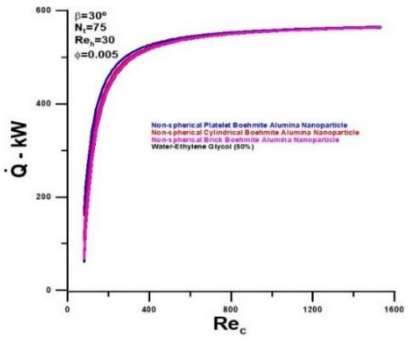

Figure 5. Heat transfer rate versus Reynolds number with volume fraction of nanoparticles equals 0.5% as parameters

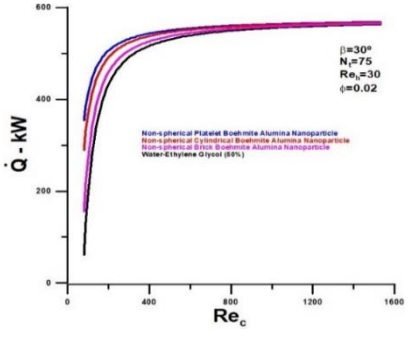

Figure 6. Heat transfer rate versus Reynolds number with volume fraction of nanoparticles equal 2.0% as parameters

However, when analyzing the results of Figures 7 and 8, the nanoparticles that present the lowest values for heat capacity ratio are Platelets, Cylindrical, and Bricks, in that order. These results can help justify the apparently contradictory results obtained for the heat transfer rate as a function of the type of nanoparticle since it is strongly influenced by the ratio between the thermal capacities, as can be seen from Equations 84 and 85. In summary, and conclusively, it can be stated that the nanoparticles that enable higher heat transfer rates are Platelets, Cylindrical, and Bricks, in that order. However, it is noteworthy that this performance difference between the nanoparticles is only observable for relatively low Reynolds numbers.

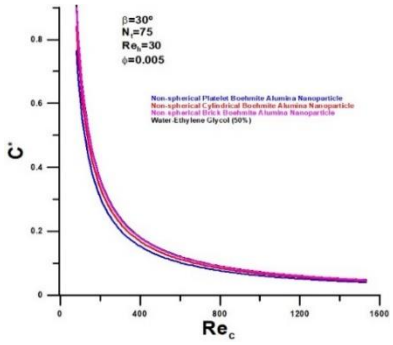

Figure 7. Thermal capacity ratio versus Reynolds number with volume fraction of nanoparticles equals 0.5% as parameters

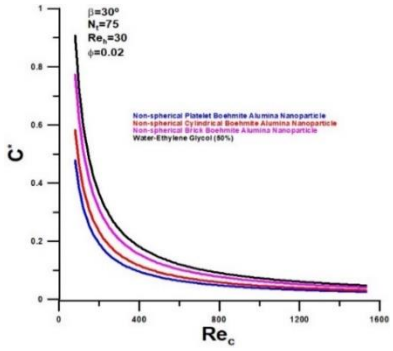

Figure 8. Thermal capacity ratio versus Reynolds number with volume fraction of nanoparticles equal 2.0% as parameters

The results obtained for the thermal entropy generation rate, through Figures 9 and 10, corroborate the conclusions related to the heat transfer rate. The Platelet-type nanoparticle has the highest rate of entropy generation, with a higher prevalence in low Reynolds number.

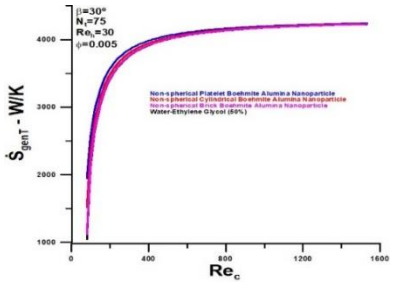

Figure 9. Thermal entropy generation rate versus Reynolds number with volume fraction of nanoparticles equals 0.5% as parameter

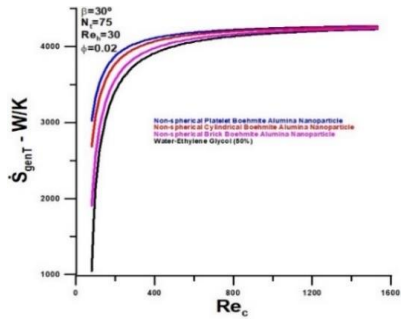

Figure 10. Thermal entropy generation rate versus Reynolds number with volume fraction of nanoparticles equal 2.0% as parameters

Figures 11 and 12 show the total pressure drop and viscous entropy generation in the heat exchanger for the volume fraction of nanoparticles equal 0.5% and 2.0%.

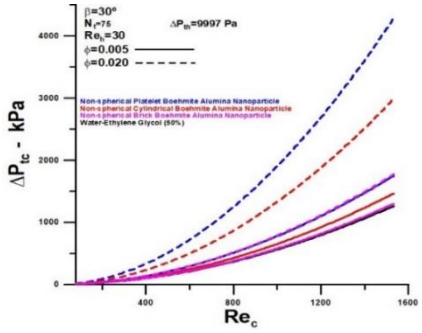

Figure 11. Total pressure drop versus Reynolds number with volume fraction of nanoparticles as parameters

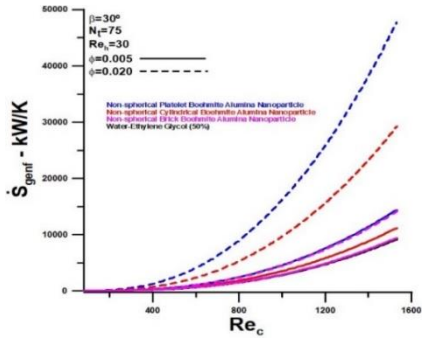

Figure 12. Viscous entropy generation versus Reynolds number with volume fraction of nanoparticles as parameters

In these cases, the influence of non-spherical nanoparticles is evident, even for the smallest fraction by volume, that is, $\phi = 0.005$. The nanoparticle that most affects the pressure drop is Platelet Boehmite Alumina, followed by Cylindrical and Brick. It becomes evident that the viscous dissipation is very high and makes the use of nanoparticles for high flow rates impractical. For lower flow rates, the use of nanoparticles is justifiable since the viscous dissipation obtained is equivalent to the viscous dissipation for a mixture of water and ethylene glycol at high flow rates.

Figure 13 highlights the relationship between thermal and viscous entropy rates, represented by the thermodynamic Bejan number, for relatively low refrigerant flows. It is evident that the thermal fraction becomes practically negligible with the increase in the flow rate of the refrigerant fluid and decreases significantly with the introduction of nanoparticles.

However, it becomes more evident in which flow rate the use of nanoparticles is feasible since the thermal portion associated with the nanoparticles is equivalent to water and ethylene glycol flow. In addition, the increase in the volume fraction further restricts the flow rate of the refrigerant fluid to be used concerning the use of nanoparticles.

Figure 14 presents the thermodynamic Bejan number variation with Reynolds number of the refrigerant fluid, with non-spherical nanoparticle Platelet volume fraction ranging from 0.5% to 2.0%. Even for the use of a mixture of water and ethylene glycol, refrigerant flows with a Reynolds number above 400 are not justified for the configuration of the heat exchanger under analysis. With the addition of nanoparticles, this maximum flow limit decreases with increasing volume fraction.

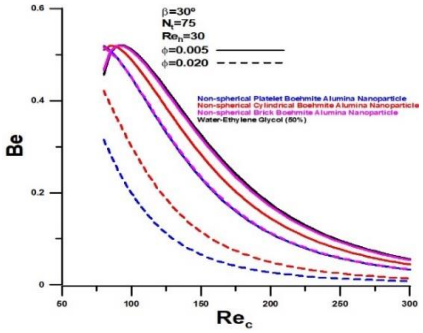

Figure 13. Bejan number versus Reynolds number with volume fraction of nanoparticles as parameters

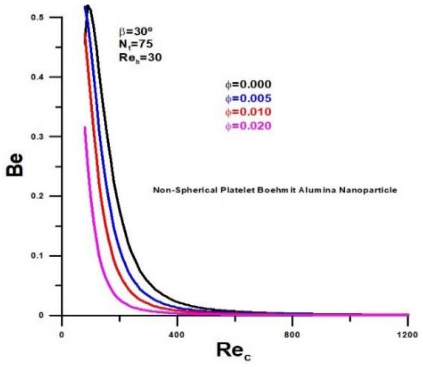

Figure 14. Bejan number versus Reynolds number with volume fraction of non-spherical platelet nanoparticle as parameters

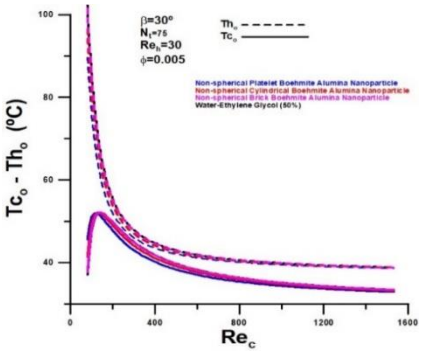

Figure 15. Outlet temperatures of fluids versus Reynolds number with volume fraction of nanoparticles equal 0.5% as parameters

Figures 15 and 16 show the temperature variations for both cold and hot fluids as a function of the Reynolds number of the refrigerant fluid and volume fractions equal to 0.5% and 2.0%, respectively. As already highlighted, the drop in temperature of the hot fluid for high flows is insignificant and not justified. With the introduction of nanoparticles, the minimum level of hot fluid outlet temperature is obtained at lower flow rates.

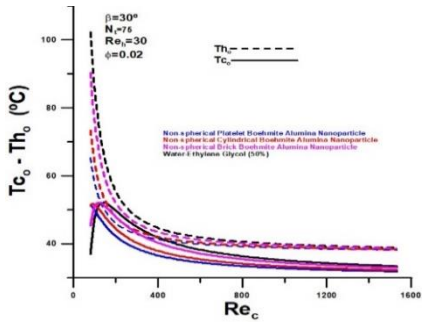

Figure 16. Outlet temperatures of fluids versus Reynolds number with volume fraction of nanoparticles equal 2.0% as parameters

Figure 17 highlights outlet temperatures for fluids using non-spherical particles of Boehmite Alumina Platelets, with volume fraction variation in the range of 0.5% to 2.0%.

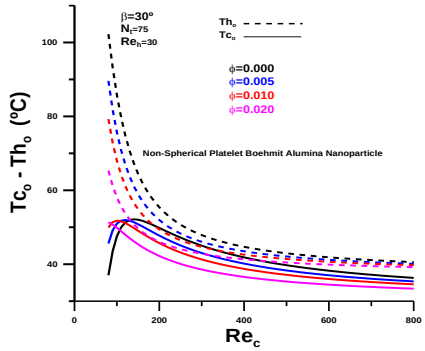

Figure 17. Outlet temperatures of fluids versus Reynolds number with volume fraction of non-spherical platelet nanoparticle as parameters

The influence of volume fractions on the drop in temperature of the hot fluid is significant and justifies the use of nanoparticles in low flow rates of the refrigerant fluid.

4. Conclusions

The work analyzes the thermohydraulic performance of a given Gasket Plate Heat Exchanger, using volume fractions of non-spherical Boehmite Alumina, through the concept of thermal and viscous entropy generation rate. The non-spherical nanoparticles under analysis are Platelets, Cylindrical and Brick.

The non-spherical nanoparticles showed higher thermal performance concerning the use of water and ethylene glycol but, on the other hand, showed higher viscous dissipations, making the use of nanoparticles in high flow rates of the refrigerant unfeasible. The highlight among the nanoparticles is non-spherical Platelets, followed by Cylindrical and Bricks.

The carried-out analysis demonstrates that the current configuration of the heat exchanger is not justified for high flow rates of the refrigerant fluid since

the drop in temperature is negligible and the price to be paid for the pressure drop is very high and grows with the introduction of nanoparticles. However, for relatively low flow rates for the coolant, the cost of viscous dissipation decreases, and the use of the current heat exchanger becomes attractive, even with volume fractions of nanoparticles in the order of 2.0%.

Conflict of interest

Authors declare no conflict of interest.

References

[1]. A.A. Neagu, C.I. Koncsag, Model validation for the heat transfer in gasket plate heat exchangers working with vegetable oils, Processes 10 (2022) 102. Doi: 10.3390/pr10010102

[2]. A.A. Neagu, C.I. Koncsag, A. Barbulescu, E. Botez, Estimation of pressure drop in gasket plate heat exchangers, Ovidius University Annals of Chemistry 27 (2016) 62-72. Doi: 10.1515/auoc-2016-0011

[3]. J. Skocilas, L. Palaziuk, CFD Simulation of the Heat Transfer Process in a Chevron Plate Heat Exchanger Using the SST Turbulence Model., Czech Technical University in Prague, Acta Polytechnica 55 (2015) 267–274. Doi: 10.14311/AP.2015.55.0267

[4]. É. Nogueira, Efficacy of the Number of Plates, Fluid Flow rate and Volume Fractions of Aluminum Oxide Nanoparticles on Thermal Performance of Gasket Plate Heat Exchanger, International Journal of Engineering Research Updates 02 (2022) 025–038. Doi: 10.53430/ijeru.2022.2.1.0027

[5]. K. Bhupal, N. Singh Shalendra, Hydraulic and thermal studies on a chevron type plate heat exchanger, Thermal Science 22 (2018) 2759-2770. Doi: 10.2298/TSCI160324312K

[6]. L. Tovazhnyanskyy, J.J. Klemeš, P. Kapustenko, O. Arsenyeva, O. Perevertaylenko, P. Arsenyev, Optimal design of welded plate heat exchanger for ammonia synthesis column: an experimental study with mathematical optimization, Energies 13 (2020) 2847. Doi: 10.3390/en13112847

[7]. M. A. Jamil, T.S. Goraya, H. Yaqoob, K.C. Ng, M.W. Shahzad, S.M. Zubair, Exergoeconomic and normalized sensitivity analysis of plate heat exchangers: a theoretical framework with application, IntechOpen, Heat Exchangers Ed. L. Castro Gomez, V.E. Velazquez Flores, M. Navarrete Procopio, pp. 1-22 (2021). Doi: 10.5772/intechopen.99736

[8]. D.H. Nguyen, K.M. Kim, T.T. Nguyen Vo, G.H. Shim, J.H. Kim, H.S. Ahn, Improvement of thermal-hydraulic performance of plate heat exchanger by electroless nickel, copper and silver plating, Case Studies in Thermal Engineering 23 (2021) 100797. Doi: 10.1016/j.csite.2020.100797

[9]. M. Monfared, A. Shahsavar, M. R. Bahrebar, Second law analysis of turbulent convection flow of boehmite alumina nanofluid inside a double-pipe heat exchanger considering various shapes for nanoparticle, Journal of Thermal Analysis and Calorimetry 135 (2019) 1521–1532. Doi: 10.1007/s10973-018-7708

[10]. S. Almurtaji, N. Ali, J.A. Teixeira, A. Addali, On the role of nanofluids in thermal-hydraulic performance of heat exchangers - A review, Nanomaterials 10 (2020) 734. Doi: 10.3390/nano10040734

[11]. E.V. Timofeeva, J.L. Routbort, D. Singh, Particle shape effects on thermophysical properties of alumina nanofluids, Journal of Applied Physics 106 (2009) 014304. Doi: 10.1063/1.3155999

[12]. O.I. Matsegora, J.J. Klemes, O.P. Arsenyeva, P.O. Kapustenko, S.K. Kusakov, V.V. Zorenko, The effect of plate corrugations geometry on performance of plate heat exchangers subjected to fouling, Chemical Engineering Transactions 76 (2019) 277-282. Doi: 10.3303/CET1976047

[13]. A. Warlo, B. Nieborg, H. Fugmann, M. Altenberend, L. Schnabel, K. Conzelmann, M. Mathieu, A. Schwärzler, Experimental Characterization of Fouling in Context of Heat Exchanger Development, Heat Exchanger Fouling and Cleaning (2019) Published online www.heatexchanger-fouling.com.

[14]. E.E. Garcia Rojas, J.S.R. Coimbra, J. Telis-Romero, Thermophysical properties of cotton, canola, sunflower and soybean oils as a function of temperature, International Journal of Food Properties 16 (2013) 1620-1629. Doi: 10.1080/10942912.2011.604889

[15]. S. Kakaç, H. Liu, A. Pramuanjaroenkij, Heat exchangers – selection, rating and thermal design, third edition, CRC Press, Taylor & Francis Groupe, Boca Raton, London, New York (2012).

[16]. W.M. Kays, A.L. London, Compact Heat Exchangers, McGraw-Hill, New York (1984).

[17]. A. Fakheri, Heat Exchanger Efficiency, Journal of Heat Transfer 129 (2007) 1268-1276. Doi: 10.1115/1.2739620

[18]. R. Tiwari, G. Maheshwari, Effectiveness and efficiency analysis of parallel flow and counter flow heat exchangers, International Journal of Application or Innovation in Engineering & Management 6 (2017) 314-319

[19]. R. Laskowski, M. Jaworski, Maximum entropy generation rate in a heat exchanger at constant inlet parameters, Journal of Mechanical and Energy Engineering 1 (2017) 71-86

[20]. A. Bejan, The thermodynamic design of heat and mass transfer processes and devices, Heat and Fluid Flow 8 (1987) 258–276. Doi: 10.1016/0142-727X(87)90062-2

Received: 02.03.2022
Received in revised form: 10.04.2022
Accepted: 11.04.2022